KINETIC SIMULATION OF UNSTEADY DETONATION WITH THERMODYNAMIC NONEQUILIBRIUM EFFECTS

Chuandong Lin[a, b], Kai H. Luo[c]

[a] Sino-French Institute of Nuclear Engineering and Technology, Sun Yat-sen University, Zhuhai 519082, China

e-mail: *linchd3@mail.sysu.edu.cn*

[b] Key Laboratory for Thermal Science and Power Engineering of Ministry of Education, Department of Energy and Power Engineering, Tsinghua University, Beijing 100084, China.

[c] Department of Mechanical Engineering, University College London, Torrington Place, London WC1E 7JE, United Kingdom

e-mail: *K.Luo@ucl.ac.uk*

ABSTRACT

Thanks to its mesoscopic kinetic nature, the discrete Boltzmann method (DBM) has the capability to investigate unsteady detonation with essential hydrodynamic and thermodynamic nonequilibrium effects. In this work, an efficient and precise reactive DBM is employed to investigate the impact of the amplitude and wave length of the initial perturbation, as well as of the chemical heat on the evolution of unsteady detonation with the nonequilibrium effects. The following conclusions have been made. (I) The initial perturbation amplitude only affects the unsteady detonation in the early period, and the detonation becomes self-similar with minor phase differences subsequently. (II) For a smaller wave length, the pressure increases faster with a higher oscillation frequency in the early period but reduces soon afterwards. The global nonequilibrium strength is larger for a smaller wave length, but is rather small when the wave length is small enough. (III) With increasing the chemical heat release, the pressure and its oscillation increase, and the nonequilibrium effect strengthens, but the oscillatory period reduces. When the wave length or chemical heat release is small enough, there is no transverse wave or cellular pattern, and the two-dimensional unsteady detonation reduces to the one-dimensional one. In this case, the maximum pressure shows a relatively weak oscillation, low average value, and long oscillatory period.

1. INTRODUCTION

Detonation is a type of compressible reactive fluid flow induced by a preshock wave, after which the chemical heat releases violently [1-3]. The shock wave coupled with a chemical reaction zone is regarded as the detonation wave propagating forwards with a supersonic speed. Detonation has wide application in engineering, industry, and safety, such as mining, gas explosion, blasting demolition, cleaning equipment, surface coating, pulse detonation engine, rotating detonation engine, etc. Due to its great importance, detonation has been studied extensively with experimental [3-8], analytical [9-13] and numerical methods [14-20] since more than a century ago. One of the earliest milestones in detonation theory is the Chapman and Jouguet (CJ) model based on conservation laws [9-10]. Another milestone is the Zeldovich-von Neumann-Döering (ZND) model, which is based on the assumption that the preshock front (as a strong discontinuity) is followed by the chemical reaction in a constant-area, inviscid, compressible flow [11-13]. These theoretical models, though being formulated for idealistic situation, continue to offer insight for more practical problems in detonation.

With the rapid development of computer hardware and computational science, numerical simulations have become indispensable for studying detonation in recent decades. The majority of numerical simulations have been carried out using macroscopic models, based on the reactive Euler or Navier-Stokes (NS) equations, which have the capability of capturing the main features of detonation, but give no detailed thermodynamic nonequilibrium information [14-16]. In contrast, microscopic methods, such as molecular dynamics, have had successes in providing detailed behaviours of detonation including nonequilibrium effects involving chemical species, at a significantly increased cost compared with macroscopic methods [19-20]. To date, mimicking the detonation process with high accuracy, efficiency and robustness remains a great challenge, because detonation involves a broad range of physicochemical phenomena, interacts over various spatial and temporal scales, contains changeable fluid interfaces, where both hydrodynamic and thermodynamic nonequilibrium effects often play essential roles [21-23].

As a central equation in kinetic theory, the Boltzmann equation has the capability of describing complex fluid flows with abundant nonequilibrium effects. However, it turns out to be particularly difficult to use the Boltzmann equation itself to solve for practical nonequilibrium situations due to its complexity in differential and integral form. To obtain their solutions, there are roughly two categories of methods. The first class is the stochastic method, including the well known direct simulation Monte Carlo [24]. Its drawbacks mainly include slow numerical convergence and random fluctuations. The second one is the deterministic simulation, such as the discrete unified gas-kinetic scheme [25], the lattice Boltzmann method [26-27], discrete Boltzmann method (DBM) [28-38], etc.

In recent years, the DBM has achieved remarkable success in simulating thermal phase separation [28-29], fluid instabilities [30-32], combustion and detonation [33-38], etc. The pioneering DBM for detonation [28], which is presented by Yan et al., is a hybrid finite

difference scheme where the discrete Boltzmann equation describes the fluid behaviour and the Lee-Tarver model controls the chemical reaction [39]. In 2016, Lin et al. proposed a double-distribution-function DBM for combustion and detonation, where one set of the discrete distribution function is for chemical reactant and the other set for product [35]. In 2019, a multiple-relaxation-time DBM is developed for detonation, where both chemical reaction and fluid flow are described by discrete Boltzmann equations.

Very recently, in the paper for the 9th International Seminar on Fire and Explosion Hazards, the DBM is preliminarily adopted to simulate the unsteady detonation with both hydrodynamic and thermodynamic nonequilibrium effects [38]. As an extended version of this paper, we carry out more in-depth and comprehensive research on unsteady detonation. In the following, the reactive DBM is introduced firstly, and three methods to obtain the reaction term are reviewed briefly. Then the DBM is employed to study the impact of perturbation amplitude, wave length, and chemical heat on the physical field of unsteady detonation with nonequilibrium effects.

2. DISCRETE BOLTZMANN METHOD FOR REACTIVE FLOWS

The DBM is based on the discrete Boltzmann equation, which is a special discretization form of the Boltzmann equation in velocity space. All physical quantities (including the density, momentum, and energy) are naturally coupled as they are described by the same one set of discrete distribution functions f_i. At the same time, the chemical reaction is associated with the fluid flow by the reaction term R_i on the right-hand side of the reactive Boltzmann equation as below,

$$\frac{\partial f_i}{\partial t}+\mathbf{v}_i\cdot\nabla f_i=\frac{1}{\tau}\left(f_i-f_i^{eq}\right)+R_i, \tag{1}$$

where t denotes the time, τ the relaxation time, f_i^{eq} the discrete equilibrium distribution function, $\mathbf{v}_i$ the discrete velocity.

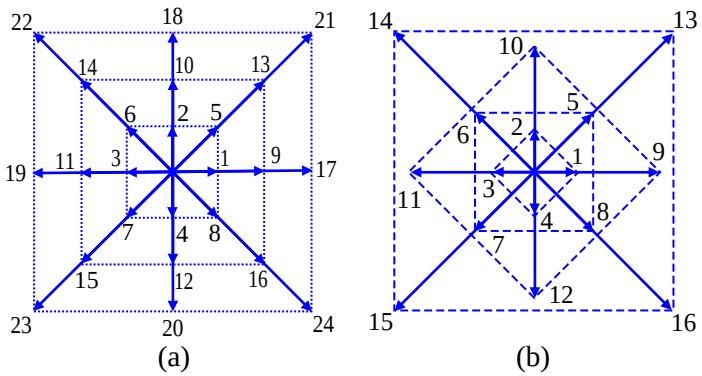

Fig. 1. Schematic of the discrete velocities: (a) D2V24 and (b) D2V16.

Figure 1 delineates two kinds of discrete velocities, two-dimensional twenty-four-velocities (D2V24) [34] and sixteen velocities (D2V16) [35-36]. To be specific, the formula of D2V24 reads [34],

$$\mathbf{v}_i = \begin{cases} v_a \overline{\mathbf{v}}_i & \text{for} \quad 1 \le i \le 8, \\ v_b \overline{\mathbf{v}}_{i-8} & \text{for} \quad 9 \le i \le 16, \\ v_c \overline{\mathbf{v}}_{i-16} & \text{for} \quad 17 \le i \le 24, \end{cases} \tag{2}$$

with

$$\overline{\mathbf{v}}_i = \begin{cases} \text{cyc:} \quad (\pm 1 \quad 0), & \text{for} \quad 1 \le i \le 4, \\ \text{cyc:} \quad (\pm 1 \quad \pm 1), & \text{for} \quad 5 \le i \le 8. \end{cases} \tag{3}$$

The mathematical expression of D2V16 takes the form [35-36],

$$\mathbf{v}_i = \begin{cases} \text{cyc}: (\pm v_a, 0) & i = 1 \sim 4, \\ \text{cyc}: (\pm v_b, \pm v_b) & i = 5 \sim 8, \\ \text{cyc}: (\pm v_c, 0) & i = 9 \sim 12, \\ \text{cyc}: (\pm v_d, \pm v_d) & i = 13 \sim 16, \end{cases} \tag{4}$$

where cyc denotes the cyclic permutation, v_a, v_b, v_c, and v_d are adjustable parameters.

To be consistent with traditional macroscopic equations in the hydrodynamic limit, it is required that f_i^{eq} and R_i satisfy the following moment relations [34],

$$\iint f^{eq} \Psi d\mathbf{v} d\eta = \sum\nolimits_i f_i^{eq} \Psi_i \ , \tag{5}$$

$$\iint R \Phi d\mathbf{v} d\eta = \sum\nolimits_i R_i \Phi_i \ , \tag{6}$$

f^{eq} and R take the form

$$f^{eq} = \frac{\rho}{2\pi T} \left(\frac{1}{2\pi I T} \right)^{1/2} \exp\left[-\frac{(\mathbf{v}-\mathbf{u}) \cdot (\mathbf{v}-\mathbf{u})}{2T} - \frac{\eta^2}{2IT} \right], \tag{7}$$

$$R = \frac{-(1+D) IT + I |\mathbf{v}-\mathbf{u}|^2 + \eta^2}{2IT^2} f^{eq} T' \ , \tag{8}$$

where ρ indicates the density, $\mathbf{u}$ the velocity, T the temperature, $T' = 2Q\lambda'/(D+I)$ the varying rate of temperature due to chemical reaction, Q the chemical heat release per unit mass of fuel, λ the mass fraction of chemical product, $D = 2$ the translational degrees of freedom, I the extra degrees of freedom due to vibration and/or rotation. In Eqs. (5) and (6), the parameters Ψ, Ψ_i, Φ and Φ_i determine the physical accuracy and computational efficiency. The more the elements, the higher the accuracy. At the level of reactive Navier-

Stokes, the minimal elements are $\Psi=1$, $\mathbf{v}$, $\left(\mathbf{v}\cdot\mathbf{v}+\eta^2\right)$, $\mathbf{vv}$, $\left(\mathbf{v}\cdot\mathbf{v}+\eta^2\right)\mathbf{v}$, $\mathbf{vvv}$, $\left(\mathbf{v}\cdot\mathbf{v}+\eta^2\right)\mathbf{vv}$, $\Psi_i=1$, $\mathbf{v}_i$, $\left(\mathbf{v}_i\cdot\mathbf{v}_i+\eta_i^2\right)$, $\mathbf{v}_i\mathbf{v}_i$, $\left(\mathbf{v}_i\cdot\mathbf{v}_i+\eta_i^2\right)\mathbf{v}_i$, $\mathbf{v}_i\mathbf{v}_i\mathbf{v}_i$, $\left(\mathbf{v}_i\cdot\mathbf{v}_i+\eta_i^2\right)\mathbf{v}_i\mathbf{v}_i$, $\Phi=1$, $\mathbf{v}$, $\left(\mathbf{v}\cdot\mathbf{v}+\eta^2\right)$, $\mathbf{vv}$, and $\Phi_i=1$, $\mathbf{v}_i$, $\left(\mathbf{v}_i\cdot\mathbf{v}_i+\eta_i^2\right)$, $\mathbf{v}_i\mathbf{v}_i$ where η and η_i corresponding to vibrational and/or rotational energies. In D2V16, the parameter $\eta_i=\eta_\alpha$, η_b, η_c, and η_d for $1\le i\le 4$, $5\le i\le 8$, $9\le i\le 12$, and $13\le i\le 16$, respectively [35-36]. In D2V24, $\eta_i=\eta_a$, η_b, and η_c, for $1\le i\le 8$, $9\le i\le 16$, and $17\le i\le 24$, respectively [34].

It is noteworthy that the DBM is capable of capturing both hydrodynamic and thermodynamic nonequilibrium [28-38]. Here let us introduce the nonequilibrium strength $\Delta=\sqrt{\sum_i \Delta_i^2}$, in terms of $\Delta_1=\sum_i f_i^{neq}$, $\Delta_2=\sum_i f_i^{neq}v_{ix}$, $\Delta_3=\sum_i f_i^{neq}v_{iy}$, $\Delta_4=\sum_i f_i^{neq}\left(v_i^2+\eta_i^2\right)$, $\Delta_5=\sum_i f_i^{neq}v_{ix}^2$, $\Delta_6=\sum_i f_i^{neq}v_{ix}v_{iy}$, $\Delta_7=\sum_i f_i^{neq}v_{iy}^2$, $\Delta_8=\sum_i f_i^{neq}\left(v_i^2+\eta_i^2\right)v_{ix}$, $\Delta_9=\sum_i f_i^{neq}\left(v_i^2+\eta_i^2\right)v_{iy}$, $\Delta_{10}=\sum_i f_i^{neq}v_{ix}^3$, $\Delta_{11}=\sum_i f_i^{neq}v_{ix}^2v_{iy}$, $\Delta_{12}=\sum_i f_i^{neq}v_{ix}v_{iy}^2$, $\Delta_{13}=\sum_i f_i^{neq}v_{iy}^3$, $\Delta_{14}=\sum_i f_i^{neq}\left(v_i^2+\eta_i^2\right)v_{ix}^2$, $\Delta_{15}=\sum_i\left(v_i^2+\eta_i^2\right)v_{ix}v_{iy}$, $\Delta_{16}=\sum_i f_i^{neq}\left(v_i^2+\eta_i^2\right)v_{iy}^2$, and $f_i^{neq}=\left(f_i-f_i^{eq}\right)$. Actually, $\Delta_1=0$ for mass conservation, $\Delta_2=\Delta_3=0$ for momentum conservation, and $\Delta_4=0$ for energy conservation. Δ_i may not equal zero for $i>4$ in a nonequilibrium state.

For the sake of simplification, the treatment of chemical reaction is based upon assumptions as follows. The chemical reaction is irreversible and exothermic. The electronic excitation, ionization and radiation are not under consideration. The chemical reaction is much slower than the relaxation process but faster than the hydrodynamic flow variation [22]. In this study, a two-step reaction scheme,

$$\xi'=Hk_I\exp\left[E_I\left(T_s^{-1}-T^{-1}\right)\right], \tag{9}$$

$$\lambda'=\left(1-H\right)k_R\left(1-\lambda\right)\exp\left(-E_RT^{-1}\right), \tag{10}$$

is adopted to mimic the essential dynamics of a chain-branching reaction [40]. In Eq. (9), ξ is the reaction progress variable in the induction period, T_s the initial shocked temperature, E_I the global activation energy describing the temperature sensitivity of the thermally neutral chemical induction process, k_I the pre-exponential factor for the ignition process, $H=H\left(\xi\right)$ a step function, i.e., $H=1$ for $\xi<1$ and $H=0$ for $\xi\ge 1$. In Eq. (10), E_R and k_R are respectively the activation energy and pre-exponential factor for the heat release process. Thus, variable ξ in Eq. (9) indicates the state of the pre-ignition process in the thermally neutral induction zone, and variable λ in Eq. (10) controls the subsequent step of the rapid energy release at and after ignition [40].

Calculation of the reaction term is the key step for the discrete Boltzmann modelling of reactive flows. Now, let us introduce three ways to obtain its mathematical expression.

(I) Type I

A straightforward method is to discretize the reaction term in the velocity space by replacing the velocity $\mathbf{v}$, the parameter η, and the equilibrium distribution function f^{eq} with their discrete counterparts $\mathbf{v}_i$, η_i, and f_i^{eq} in Eq. (8), we get the discrete form of the reaction term as below,

$$R_i = \frac{-\left(1+D\right)IT + I\left|\mathbf{v}_i - \mathbf{u}\right|^2 + \eta_i^2}{2IT^2} f_i^{eq} T' \ . \tag{11}$$

Obviously, the expansion in the above equation contains factors $\left|\mathbf{v}_i - \mathbf{u}\right|^2 f_i^{eq}$ and $\eta_i^2 f_i^{eq}$. Hence, to ensure that the discrete reaction term obeys the moment relations in Eq. (6), the elements $\Psi = \eta^2 \mathbf{vv}$, $\left(\mathbf{v}\cdot\mathbf{v}+\eta^2\right)\eta^2$, $\left(\mathbf{v}\cdot\mathbf{v}+\eta^2\right)\mathbf{v}\cdot\mathbf{vv}$, $\left(\mathbf{v}\cdot\mathbf{v}+\eta^2\right)\eta^2\mathbf{v}$, and corresponding $\Psi_i = \eta_i^2 \mathbf{v}_i\mathbf{v}_i$, $\left(\mathbf{v}_i\cdot\mathbf{v}_i+\eta_i^2\right)\eta_i^2$, $\left(\mathbf{v}_i\cdot\mathbf{v}_i+\eta_i^2\right)\mathbf{v}_i\cdot\mathbf{v}_i\mathbf{v}_i$, $\left(\mathbf{v}_i\cdot\mathbf{v}_i+\eta_i^2\right)\eta_i^2\mathbf{v}_i$ should be included in Eq. (5) in addition to the aforementioned minimal elements. Actually, these relations are all satisfied in the D2V24 [34].

(II) Type II

An alternative approach is to compute the reaction term based on its physical definition [35-36]. Specifically, the reaction term is the variation rate of the distribution function due to the chemical reaction,

$$R_i = \frac{1}{\tau}\left(f_i^{*eq} - f_i^{eq}\right) , \tag{12}$$

where $f_i^{eq} = \left(\rho,\ \mathbf{u},\ T\right)$ and $f_i^{*eq} = \left(\rho,\ \mathbf{u},\ T^*\right)$ denote the discrete equilibrium distribution function before and after the chemical reaction, respectively. Since the chemical reaction is much faster than the hydrodynamic flow variations [22], neither density nor flow velocity changes during a relatively small time interval of chemical reaction, while the temperature is affected by the chemical heat, i.e., $T^* = T + \tau T'$.

(III) Type III

A direct way to calculate the reaction term is by the matrix inversion method [37-38]. Specifically, Eq. (6) can be uniformly rewritten as

$$\mathbf{M_R} = \mathbf{CR} , \tag{13}$$

where $\mathbf{R}=\left(R_1 \quad R_2 \quad \cdots \quad R_{16}\right)^{\mathrm{T}}$ represents the set of discrete reaction terms, $\mathbf{M_R}=\left(M_{R1} \quad M_{R2} \quad \cdots \quad M_{R16}\right)^{\mathrm{T}}$ the set of kinetic moments, and $\mathbf{C}$ a square matrix linking the velocity space to moment space. The elements of $\mathbf{M_R}$ are $M_{R1}=0$, $M_{R2}=0$, $M_{R3}=0$, $M_{R4}=\rho\left(D+I\right)T'$, $M_{R5}=\rho T'$, $M_{R6}=0$, $M_{R7}=\rho T'$, $M_{R8}=\left(D+I+2\right)\rho u_x T'$, $M_{R9}=\left(D+I+2\right)\rho u_y T'$, $M_{R10}=3\rho u_x T'$, $M_{R11}=\rho u_y T'$, $M_{R12}=\rho u_x T'$, $M_{R13}=3\rho u_y T'$, $M_{R14}=\rho\left[2T\left(D+I+2\right)+\left(D+I+5\right)u_x^2+u_y^2\right]T'$, $M_{R15}=\rho u_x u_y\left(D+I+4\right)T'$, $M_{R16}=\rho\left[2T\left(D+I+2\right)+u_x^2+\left(D+I+5\right)u_y^2\right]T'$. The elements of $\mathbf{C}$ are $C_{1i}=1$, $C_{2i}=v_{ix}$, $C_{3i}=v_{iy}$, $C_{4i}=v_i^2+\eta_i^2$, $C_{5i}=v_{ix}^2$, $C_{6i}=v_{ix}v_{iy}$, $C_{7i}=v_{iy}^2$, $C_{8i}=\left(v_i^2+\eta_i^2\right)v_{ix}$, $C_{9i}=\left(v_i^2+\eta_i^2\right)v_{iy}$, $C_{10i}=v_{ix}^3$, $C_{11i}=v_{ix}^2v_{iy}$, $C_{12i}=v_{ix}v_{iy}^2$, $C_{13i}=v_{iy}^3$, $C_{14i}=\left(v_i^2+\eta_i^2\right)v_{ix}^2$, $C_{15i}=\left(v_i^2+\eta_i^2\right)v_{ix}v_{iy}$, $C_{16i}=\left(v_i^2+\eta_i^2\right)v_{iy}^2$. Hence, the discrete reaction term is obtained as below [37-38]

$$\mathbf{R}=\mathbf{C}^{-1}\mathbf{M_R}\ . \tag{14}$$

It is noteworthy that type I has 9 moment relations satisfied by the reaction term, requiring 24 moment relations satisfied by the discrete equilibrium distribution function, and the D2V24 is employed correspondingly [34]. For types II and III, there are 16 moment relations satisfied by both the discrete equilibrium distribution function and reaction term, and, consequently, the D2V16 is utilized. Moreover, type II is at the level of the first-order temporal accuracy [35-36]. Therefore, type III [37-38] is physically more accurate and numerically more precise than the types I and II. In this paper, type III is adopted for numerical simulations.

3. SIMULATION OF UNSTEADY DETONATION

In this section, the DBM is adopted to simulate and investigate the unsteady detonation with both hydrodynamic and thermodynamic nonequilibrium effects. The computational domain, with the area $L_x\times L_y$, is divided into two parts. The burnt and fresh gas compositions are imposed on the left L and right R parts, respectively. The fresh gas flows into the domain from the right side, and the burnt gas flows out from the left boundary. The simulation domain is bounded by an outlet (inlet) boundary condition on the left (right) side and periodic boundary conditions in the vertical direction. The initial physical field takes the form,

$$\begin{cases}\rho=\dfrac{\rho_L+\rho_R}{2}-\dfrac{\rho_L-\rho_R}{2}\tanh\left(\dfrac{x-x_0}{W}\right),\\ T=\dfrac{T_L+T_R}{2}-\dfrac{T_L-T_R}{2}\tanh\left(\dfrac{x-x_0}{W}\right),\\ \mathbf{u}=\dfrac{\mathbf{u}_L+\mathbf{u}_R}{2}-\dfrac{\mathbf{u}_L-\mathbf{u}_R}{2}\tanh\left(\dfrac{x-x_0}{W}\right),\end{cases} \tag{15}$$

with quantities (ρ_L, T_L, $\mathbf{u}_L$) = (1.48043, 2.06314, −1.69953$\mathbf{e}_x$) and (ρ_R, T_R, $\mathbf{u}_R$) = (1, 1, −2.51603$\mathbf{e}_x$). The hyperbolic tangent function, tanh, is used to smooth the interface between the two parts in the computational domain, and the layer width is $W = L_x/150$. In order to trigger the unsteady flow, a perturbation of a sine curve $x_0 = L_x/10 - A\cos(ky)$ is imposed on the interface, with an amplitude A and wave number $k = 2\pi/L_y$, where the wave length is equal to L_y . The schematic of the initial configuration for subsequent simulation of the unsteady detonation is shown in Fig. 2.

It should be noted that the evolution of unsteady detonation is practically important in the fields of industrial explosion safety, mining and detonation propulsion, etc. The unsteady characteristics are usually associated with spatial and temporal inhomogeneities, such as inhomogeneous concentrations, temperature gradients, flow variations, non-uniform geometries, introduced by many factors in storage, transportation and working conditions. Such inhomogeneities play a significant role in the entire process of detonation starting from the initiation. To represent such effects, we introduce initial perturbations in the imposed amplitude and wave length.

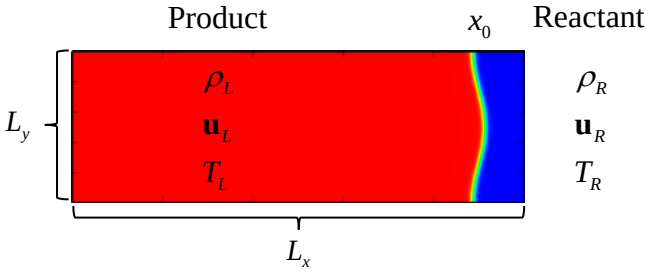

Fig. 2. Schematic of the initial configuration for simulation of unsteady detonation.

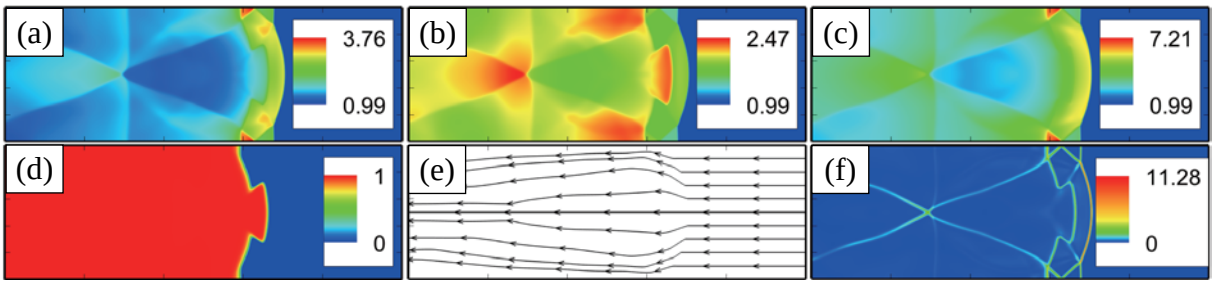

Fig. 3. Contours of density (a), temperature (b), pressure (c), reaction progress variable (d), streamline (e), and nonequilibrium strength (f) at the time $t = 0.1$ in the detonation process.

Figure 3 illustrates physical quantities (density, temperature, pressure, reaction progress variable, streamline, and nonequilibrium strength) at a time instant in the process of the unsteady detonation. It is evident in Figs. 3 (a)-(c) that the density, temperature, and pressure increase abruptly from right to left around the pre-shocked front due to the compressible effects. Afterward, as shown in Fig. 3 (d), the chemical reaction takes place, and the chemical

energy releases violently in the reaction zone. Figure 3 (e) shows that the flow direction (as well as the velocity magnitude) is significantly affected by the pre-shocked front and transverse waves that enhance the detonation instability. The transverse waves collide periodically behind the pre-shocked wave and generate peaks of pressure and temperature in the product zone. Comparison between panels (a)-(e) and (f) indicates that the nonequilibrium effect is strong near the pre-shock front, transverse wave, and Mach stem, where physical gradients are quite sharp. Consequently, the nonequilibrium manifestation could be employed to probe the fine structures of the unsteady detonation. It is indeed quite easy to identify the pre-shock wave, the transverse wave, the reaction zone, the triple point, and the cellular structure in panel (f). The triple point is located at the junction of the pre-shock front, Mach stem, and transverse wave, and its spatiotemporal trajectory is actually a cellular pattern.

3.1. Impact of perturbation amplitude

Figure 4 exhibits the maximum pressure and global nonequilibrium strength in the evolution of unsteady detonation with various initial perturbation amplitudes. Figures 4 (a) and (b) illustrate the maximum pressure within time periods $0.0075 \le t \le 0.018$ and $0.091 \le t \le 0.1$, respectively. Figures 4 (c) and (d) plot the global nonequilibrium strength within time periods $0.0075 \le t \le 0.018$ and $0.091 \le t \le 0.1$, respectively. The global nonequilibrium strength is $\iint \Delta dxdy$ where the integral is extended over the whole computational region $L_x \times L_y$.

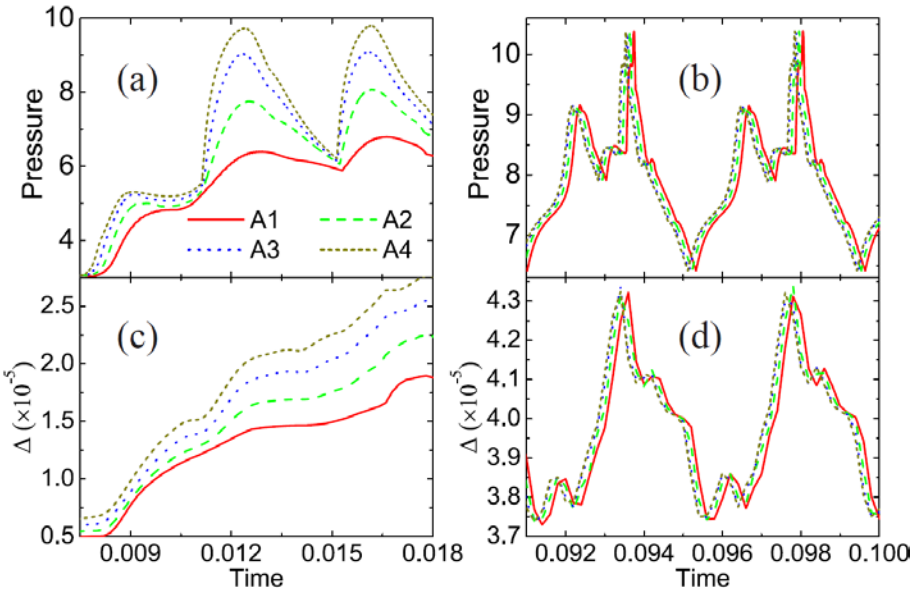

Fig. 4. The maximum pressure and nonequilibrium strength in the evolution of detonation with various perturbation amplitudes. The solid, dashed, dotted and short-dashed lines represent the initial perturbation amplitudes $A_1 = L_y/100$, $A_2 = L_y/50$, $A_3 = L_y/25$, $A_4 = L_y/12.5$, respectively.

It can be found in Figs. 4 (a) and (c) that, in the primary period, both the maximum pressure and global nonequilibrium strength are larger for a larger initial perturbation amplitude, and the maximum pressure has different oscillations under various initial perturbations. It is clear in Figs. 4 (b) and (d) that, in the later period, the physical fields change periodically and similarly with only some phase differences under various initial perturbation amplitudes. Therefore, the initial perturbation amplitude only impacts on the formation of the unsteady self-sustained detonation in the early period. Afterward, the amplitude or shape of the initial perturbation is "forgotten" gradually, and the detonation becomes self-similar with only a phase difference in the later process. Physically, everything left behind the sonic or supersonic front is "forgotten" after the stabilization of a detonation wave, which is different from a subsonic wave (i.e. flame) whose formation and evolution are affected by the initial perturbation in the whole process.

3.2. Impact of wave length

To study the effect of the wave length of initial perturbation on the detonation process, we take into account four cases with wave lengths $L_{y1}=2.5\times10^{-3}$, $L_{y2}=5\times10^{-3}$, $L_{y3}=10^{-2}$, and $L_{y4}=2\times10^{-2}$. Figure 5 illustrates the contours of nonequilibrium strength at the time $t=0.1$ in the detonation process with various wave lengths of initial perturbation. It can be found that the maximum nonequilibrium strength increases with the increasing wave length, because the maximum physical gradient is larger for a larger wave length. Moreover, the cellular size becomes smaller for a smaller wave length. As shown in Fig. 5 (a), the transverse wave and cellular pattern disappear when the wave length is small enough.

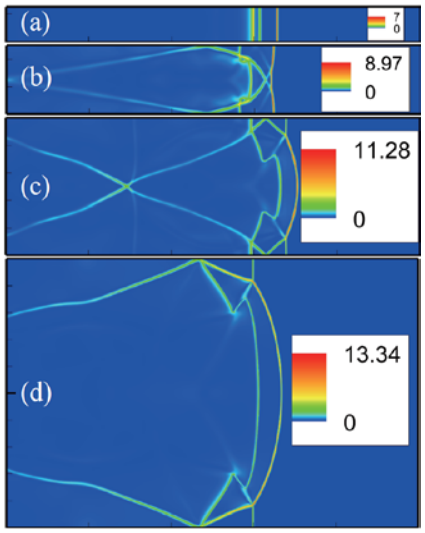

Fig. 5. Contours of nonequilibrium strength at the time $t = 0.1$ in the detonation process with various wave lengths: (a) $L_{y1} = 2.5\times10^{-3}$, (b) $L_{y2} = 5\times10^{-3}$, (c) $L_{y3} = 10^{-2}$, and (d) $L_{y4} = 2\times10^{-2}$.

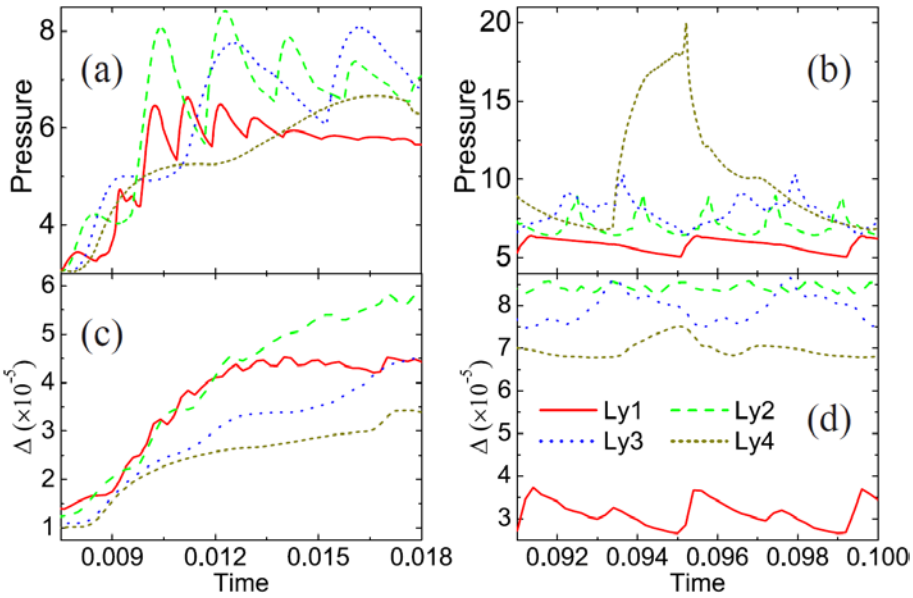

Fig. 6. The maximum pressure and nonequilibrium strength in the evolution of detonation with various wave lengths. The solid, dashed, dotted and short-dashed lines represent the wave length $L_{y1} = 2.5\times10^{-3}$, $L_{y2} = 5\times10^{-3}$, $L_{y3} = 10^{-2}$, and $L_{y4} = 2\times10^{-2}$, respectively.

To have a quantitative study of the wave length on the detonation process, we plot the evolution of the maximum pressure and nonequilibrium strength under the condition of various wave lengths. Figure 6 displays the evolution of global nonequilibrium strength

$\omega\iint \Delta dxdy$, with $\omega = 8$, 4, 2, and 1 for the cases with $L_{y1} = 2.5\times10^{-3}$, $L_{y2} = 5\times10^{-3}$, $L_{y3} = 10^{-2}$, and $L_{y4} = 2\times10^{-2}$, respectively. Here the parameter ω is used to make the integral extended over the same computational region. It is clear in Figs. 6 (a)-(b) that, for a smaller wave length, the pressure increases faster with a higher oscillation frequency in the early period, reduces earlier afterward, and becomes smaller in the later stage. In particular, in the case when the wave length is small enough, the two-dimensional unsteady detonation reduces to the one-dimensional unsteady detonation. The maximum pressure exhibits relatively small oscillations, low average value, and long oscillatory period. Moreover, from Figs. 6 (c)-(d), we can find that the global nonequilibrium strength is larger for a smaller wave length, but is rather small when the wave length is small enough. Mathematically, global nonequilibrium strength is a function of local nonequilibrium strength and the nonequilibrium area. With reducing wave length, the physical gradients reduce, hence the local nonequilibrium strength decreases. On the other hand, the nonequilibrium area increases with decreasing wave length. Consequently, there is a competition between the reducing physical gradients and increasing nonequilibrium area, and the global nonequilibrium strength increases as the increasing nonequilibrium area dominates. Both local nonequilibrium strength and area become small when the wave length is small enough.

3.3. Impact of chemical heat

Finally, the impact of chemical heat release on the evolution of detonation is investigated. We perform simulations with various chemical heat releases of $Q = 0.5$, 1.0, 1.5, and 2.0. Figure 7 exhibits contours of nonequilibrium strength at the time $t = 0.1$ in the detonation process. It is clear that the case with $Q = 0.5$ is significantly different from the other three cases with $Q = 1.0$, 1.5, and 2.0 that are similar with periodic evolution of transverse wave and cellular pattern. There is no transverse wave or cellular pattern when the chemical heat release is small enough, as shown in Fig. 7 (a). Furthermore, with the increase of chemical heat, the nonequilibrium strength increases. The detonation becomes more violent, and the physical gradients are sharper for a larger value of chemical heat. Mathematically, the nonequilibrium effect is larger for a larger value of either physical gradient or chemical heat [35].

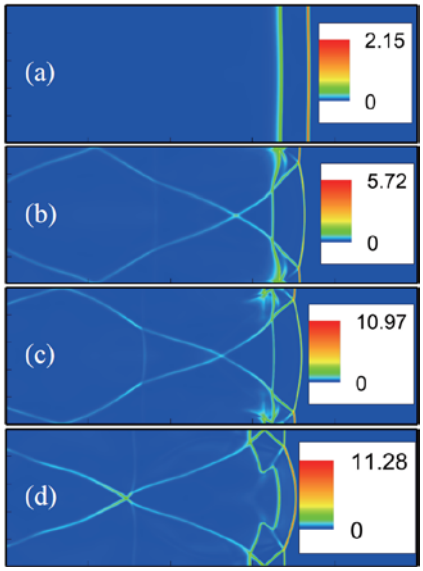

Fig. 7. Contours of nonequilibrium strength at the time $t = 0.1$ in the detonation process with various values of chemical heat release: (a) $Q = 0.5$, (b) $Q = 1.0$, (c) $Q = 1.5$, and (d) $Q = 2.0$

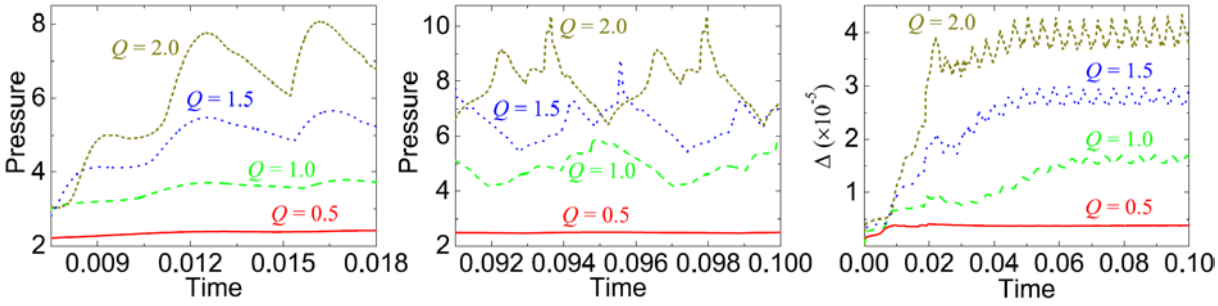

(a) (b) (c)

Fig. 8. The maximum pressure (a, b) and global nonequilibrium strength (c) in the evolution of detonation with various values of chemical heat release

Figure 8 illustrates the evolution of the maximum pressure and global nonequilibrium strength $\iint \Delta dxdy$, where the integral is extended over the whole physical region. It is evident that both quantities are higher for larger chemical heat release. They display periodic oscillations as the time goes on, and the periods are 0.0059, 0.0051, 0.0046, and 0.0043, for cases with $Q = 0.5$, 1.0, 1.5, and 2.0, respectively. Therefore, the period reduces with increasing chemical heat. The magnitude of the oscillations increases with the chemical heat release.

CONCLUSIONS

As a mesoscopic kinetic method, the DBM has the capability to simulate unsteady detonation with both hydrodynamic and thermodynamic nonequilibrium effects beyond traditional

macroscopic fluid models. The fluid flow and chemical reaction are naturally coupled via the reaction term on the right-hand side of the discrete Boltzmann equation. Three types of methods are introduced to obtain the reaction term: (i) to discretize the original reaction term in the velocity space, (ii) to compute the reaction term on the basis of its physical definition, and (iii) to calculate the reaction term with the matrix inversion method. The last approach, which is physically more accurate and numerically more precise [37-38], has been adopted to investigate the nonequilibrium effects in the unsteady detonation process.

The impact of perturbation amplitude, wave length, and chemical heat on the evolution of detonation is studied in detail. The following results have been obtained.

(I) The initial perturbation amplitude or shape only impacts on the formation of the unsteady self-sustained detonation during the initial period.

(II) For a smaller wave length of the initial perturbation, the pressure increases faster with a higher oscillation frequency in the early period, but reduces earlier afterwards, and becomes smaller in the later stage. The global nonequilibrium strength is larger for a smaller wave length, but is rather smaller when the wave length is small enough. In this case, the maximum pressure shows a relatively small oscillation, low average value, and long oscillatory period.

(III) With increasing chemical heat release, the pressure and its oscillation increase, and the nonequilibrium effect strengthens as well, while the oscillatory period reduces.

(IV) If the wave length of the initial perturbation or chemical heat release is small enough , there is no transverse wave or cellular pattern, and the two-dimensional unsteady detonation reduces to the one-dimensional one.

ACKNOWLEDGEMENT

This work is supported by the Natural Science Foundation of China (NSFC) under Grant Nos. 91441120 and 51806116. Support from the UK Engineering and Physical Sciences Research Council under the project “UK Consortium on Mesoscale Engineering Sciences (UKCOMES)” (Grant No. EP/R029598/1) is gratefully acknowledged.

REFERENCES

1. C. K. Law, Combustion Physics (Cambridge University Press, Cambridge, 2006).
2. C. A. Handley, B. D. Lambourn, N. J. Whitworth, et al. “Understanding the shock and detonation response of high explosives at the continuum and meso scales,” Appl. Phys. Rev., **5**(1) 011303 (2018).
3. W. Fickett, W. C. Davis, Detonation: theory and experiment (Dover Publications, New York, 2000).
4. M. I. Radulescu, J. H. S. Lee. “The failure mechanism of gaseous detonations: experiments in porous wall tubes,” Combust. Flame, **131**(1-2): 29-46 (2002).

5. Y. Gao, H. D. Ng, J. H. S. Lee. “Experimental characterization of galloping detonations in unstable mixtures,” Combust. Flame, **162**(6): 2405-2413 (2015).

6. B. M. N. Maxwell, R. R. Bhattacharjee. “Lau-Chapdelaine S S M, et al. Influence of turbulent fluctuations on detonation propagation,” J. Fluid Mech., 818: 646-696 (2017).

7. J. Li, H. Ren, X. Wang, et al. “Length scale effect on Mach reflection of cellular detonations,” Combust. Flame, 189: 378-392 (2018).

8. Z. Pan, K. Chen, J. Qi, et al. “The propagation characteristics of curved detonation wave: Experiments in helical channels,” Proc. Combust. Inst., **37**(3): 3585-3592 (2019).

9. D. L. Chapman. “On the rate of explosion in gases,” Philos. Mag., **47**(284): 90-104 (1899).

10. E. Jouguet. “On the propagation of chemical reactions in gases,” J. Math. Pures Appl., **1**: 347-425 (1905).

11. Y. B. Zeldovich. “On the theory of the propagation of detonation in gaseous systems,” J. Exp. Theor. Phys. **10**: 542-568 (1940).

12. J. von Neumann. “Theory of detonation waves,” Macmillan, New York, 1942.

13. W. Döering. “On detonation processes in gases,” Ann. Phys. **435**: 421-436, 1943.

14. J. E. Shepherd. “Detonation in gases,” Proc. Combust. Inst., **32**(1): 83-98 (2009).

15. W. Han, Y. Gao, C. K. Law. “Flame acceleration and deflagration-to-detonation transition in micro-and macro-channels: An integrated mechanistic study,” Combust. Flame, 176: 285-298 (2017).

16. H. Xiao, E. S. Oran. “Shock focusing and detonation initiation at a flame front,” Combust. Flame, **203**: 397-406 (2019).

17. Peyrard M, Odiot S, Oran E, et al. “Microscopic model for propagation of shock-induced detonations in energetic solids,” Phys. Rev. B, **33**(4): 2350 (1986).

18. D. Guo, D. Guo, F. Huang, et al. “Influence of Silicon on the Detonation Performance of Energetic Materials from First-Principles Molecular Dynamics Simulations,” J. Phys. Chem. C, **122** (42): 24481-24487 (2018).

19. C. M. Tarver, J. W. Forbes, P. A. Urtiew. “Nonequilibrium Zeldovich-von Neumann-Doring theory and reactive flow modeling of detonation,” Russ. J. Phys. Chem. B, **1**(1): 39-45 (2007).

20. E. Nagnibeda, E. Kustova. Non-equilibrium reacting gas flows: kinetic theory of transport and relaxation processes (Springer, Berlin, 2009).

21. K. C. K. Uy, L. S. Shi, C. Y. Wen. “Prediction of half reaction length for H2O2Ar detonation with an extended vibrational nonequilibrium Zel'dovich-von Neumann-Döring (ZND) model,” Int. J. of Hydrogen Energy, **44**(14): 7667-7674 (2019).

22. J. B. Anderson, L. N. Long. “Direct Monte Carlo simulation of chemical reaction systems: Prediction of ultrafast detonations,” J. Chem. Phys., **118**(7): 3102-3110 (2003).

23. C. Wu, B. Shi, Z. Chai, et al. “Discrete unified gas kinetic scheme with a force term for incompressible fluid flows,” Comput. Math. Appl., **71**(12): 2608-2629 (2016).

24. J. Meng, Y. Zhang, N. G. Hadjiconstantinou, et al. “Lattice ellipsoidal statistical BGK model for thermal non-equilibrium flows,” J. Fluid Mech., **718**: 347-370 (2013).

25. S. A. Hosseini, N. Darabiha, D. Thévenin. “Lattice Boltzmann advection-diffusion model for conjugate heat transfer in heterogeneous media,” Int. J. Heat Mass Transfer, **132**: 906-919 (2019).

26. Y. Gan, A. Xu, G. Zhang, et al. “Discrete Boltzmann modeling of multiphase flows: hydrodynamic and thermodynamic non-equilibrium effects,” Soft Matter, **11**(26): 5336-5345 (2015).

27. Y. Zhang, A. Xu, G. Zhang, et al. “Entropy production in thermal phase separation: a kinetic-theory approach,” Soft matter, **15**(10): 2245-2259 (2019).

28. H. Lai, A. Xu, G. Zhang, et al. “Nonequilibrium thermohydrodynamic effects on the Rayleigh-Taylor instability in compressible flows,” Phys. Rev. E, **94**(2): 023106 (2016).

29. F. Chen, A. Xu, G. Zhang. “Collaboration and competition between Richtmyer-Meshkov instability and Rayleigh-Taylor instability,” Phys. Fluids, **30**(10): 102105 (2018).

30. Y. B. Gan, A. G. Xu, G. C. Zhang, et al. “Nonequilibrium and morphological characterizations of Kelvin-Helmholtz instability in compressible flows,” Front. Phys., **14**(4): 43602 (2019).

31. B. Yan, A. Xu, G. Zhang, et al. “Lattice Boltzmann model for combustion and detonation,” Front. Phys., **8**(1): 94-110 (2013).

32. A. Xu, C. Lin, G. Zhang, et al. “Multiple-relaxation-time lattice Boltzmann kinetic model for combustion,” Phys. Rev. E, **91**(4): 043306 (2015).

33. C. Lin, A. Xu, G. Zhang, et al. “Double-distribution-function discrete Boltzmann model for combustion,” Combust. Flame, **164**: 137-151 (2016).

34. C. Lin, K. H. Luo, L. Fei, et al. “A multi-component discrete Boltzmann model for nonequilibrium reactive flows,” Sci. Rep., **7**(1): 14580 (2017).

35. C. Lin, K. H. Luo. “Discrete Boltzmann modeling of unsteady reactive flows with nonequilibrium effects,” Phys. Rev. E, **99**(1): 012142 (2019).

36. C. Lin, K. H. Luo. “Kinetic simulation of unsteady detonation with nonequilibrium effects,” Proceedings of the 9th International Seminar on Fire and Explosion Hazards (ISFEH9), St. Petersburg Polytechnic University Press, pp. 289-300 (2019).

37. T. Lee, C. Lin, L. Chen. “A lattice Boltzmann algorithm for calculation of the laminar jet diffusion flame,” Journal of Computational Physics, **215**(1): 133-152 (2006).

38. H. D. Ng, M. I. Radulescu, A. J. Higgins, et al. “Numerical investigation of the instability for one-dimensional Chapman-Jouguet detonations with chain-branching kinetics,” Combust. Theor. Model., **9**(3): 385-401 (2005).

450

451